

NEUROSYSTEMS

Distinct local circuit properties of the superficial and intermediate layers of the rodent superior colliculus

Penphimon Phongphanphanee,^{1,*} Robert A. Marino,² Katsuyuki Kaneda,^{1,3,†} Yuchio Yanagawa,^{4,5} Douglas P. Munoz² and Tadashi Isa^{1,3,5}

¹Department of Developmental Physiology, National Institute of Physiological Sciences, Myodaiji, Okazaki 444-8585, Japan

²Centre for Neuroscience Studies, Queen's University, Kingston, ON, Canada

³Department of Physiological Sciences, School of Life Science, The Graduate University for Advanced Studies (SOKENDAI), Hayama, Japan

⁴Department of Genetics and Behavioral Neurosciences, Gunma University Graduate School of Medicine, Maebashi, Japan

⁵The Core Research for Evolutionary Science and Technology (CREST), Japan Science and Technology Agency (JST), Kawaguchi, Japan

Keywords: inhibition, lateral interactions, mouse, patch clamp, saliency

Abstract

The superior colliculus (SC) is critical in localizing salient visual stimuli and making decisions on the location of the next saccade. Lateral interactions across the spatial map of the SC are hypothesized to help mediate these processes. Here, we investigate lateral interactions within the SC by applying whole-cell recordings in horizontal slices of mouse SC, which maintained the local structure of the superficial (SCs) visual layer, which is hypothesized to participate in localizing salient stimuli, and the intermediate (SCi) layer, which is supposed to participate in saccade decision-making. When effects of either electrical or chemical (uncaging of free glutamate) stimuli were applied to multiple sites with various distances from the recorded cell, a pattern of center excitation-surround inhibition was found to be prominent in SCs. When the interactions of synaptic effects induced by simultaneous stimulation of two sites were tested, non-linear facilitatory or inhibitory interactions were observed. In contrast, in the SCi, stimulation induced mainly excitation, which masked underlying inhibition. The excitatory synaptic effects of stimulation applied at remote sites were summed in a near linear manner. The result suggested that SCs lateral interactions appear suitable for localizing salient stimuli, while the lateral interactions within SCi are more suitable for faithfully accumulating subthreshold signals for saccadic decision-making. Implementation of this laminar-specific organization makes the SC a unique structure for serially processing signals for saliency localization and saccadic decision-making.

Introduction

The visual world provides a rich mix of complex and dynamic stimuli, not all of which can be viewed by the high-acuity fovea. Therefore, a selection process, which works via lateral interactions between competing stimuli across the visual field, is required for determining the goal for gaze shifts (Buswell, 1935; Yarbus, 1967). However, it is still unknown which brain structures implement such competitive processes. One likely area is the superior colliculus (SC), a midbrain structure critical for computing saliency, controlling saccades and spatial attention (Sparks, 1986, 2002; Gandhi & Katnani, 2011; White & Munoz, 2011; Krauzlis *et al.*, 2013). The superficial

layers (SCs) receive convergent visual input from visual structures (e.g. retina, visual cortex), and the intermediate layers (SCi) are interconnected with parietal and frontal cortex, and with the basal ganglia (Sparks, 1986; Gandhi & Katnani, 2011; Krauzlis *et al.*, 2013). These layers contain topographical representations of visual (SCs) and motor (SCi) space (Robinson, 1972; Schiller & Stryker, 1972).

Evidence for lateral interactions was derived from experiments using extracellular recording and electrical stimulation in awake monkeys (Munoz & Istvan, 1998) and in SC slices from ferrets (Meredith & Ramoa, 1998). Other studies have shown the presence of excitatory and inhibitory commissural neurons in the cat (Behan, 1985; Olivier *et al.*, 2000; Takahashi *et al.*, 2007). Models of target selection have used the collicular map and implemented local excitatory and remote inhibitory interactions (Arai *et al.*, 1999; Trappenberg *et al.*, 2001; Badler & Keller, 2009; Marino *et al.*, 2012).

In contrast, other studies do not attribute such competitive processes in the SC. A number of neurons over a large region of the SC are activated preceding saccades and their goal is determined by the center of gravity of the activated population (Lee *et al.*, 1988) and vector-averaging between two saccade goals (Edelman & Keller,

Correspondence: Dr T. Isa, ¹Department of Developmental Physiology, as above.
E-mail: tisa@nips.ac.jp

**Present address:* Pharmaceutical Division, Novartis (Thailand) Limited, 622 Emporium Tower, 15th Floor, Sukhumvit Road, Klongton, Klongtoey, Bangkok 10110, Thailand

†*Present address:* Department of Pharmacology, Graduate School of Pharmaceutical Sciences, Hokkaido University, Kita-12 jo-Nishi-6 chome, Sapporo 060-0812, Japan

Received 5 January 2014, revised 4 March 2014, accepted 5 March 2014

1998). Furthermore, *in vitro* experiments using SC slices failed to identify long-range lateral interactions (Lee & Hall, 2006). How could such contrasting arguments be reconciled? The SC is a multi-layered structure and it has been suggested that the SCs has the cytoarchitecture of a sensory area, while that of SCi is more similar to the reticular formation (Edwards, 1980). The density of the GABAergic neurons also differs between the two layers, with the density being much higher (> 50%) in the SCs (Mize, 1992). Therefore, the organization of lateral connections within each layer may be different because they participate in different processes.

To study the lateral interaction in SCs and SCi independently, we established a novel experimental preparation, horizontal slices of mouse SC, in which the structure of local lateral connections is preserved. Horizontal interactions were studied by applying electrical or chemical stimulation to locations across the SC map to identify local synaptic connections. In addition, the effect of simultaneous stimulation of two sites was investigated to mimic the competition among multiple potential targets in visual space. We provide compelling evidence of significant differences in lateral interactions between SCs and SCi, which reconcile the concurrent arguments on the role of the SC in saliency localization and target selection.

Methods

The experimental protocol followed the guidelines for animal experimentation established by the Ministry of Education, Culture, Sports, Science and Technology of Japan and was approved by the Animal Research Committee of the National Institutes of Natural Sciences.

Slice preparations

Procedures for slice preparation were described previously (Isa *et al.*, 1998). Briefly, horizontal slices (250 μm thick) of the SC were prepared from GAD67-GFP knock-in mice (Tamamaki *et al.*, 2003) that were 16–20 days of age. We used this line of mice so that we could visualize GABAergic neurons prior to recording (Endo *et al.*, 2003; Tamamaki *et al.*, 2003; Kaneko *et al.*, 2008). In this report, we describe the results of recordings from non-GABAergic neurons, which constitute the majority of projection neurons (Endo *et al.*, 2003; Sooksawate *et al.*, 2005). The animals were deeply anesthetized with ether and decapitated. Brains were quickly removed and submerged in ice-cold modified Ringer solution containing (in mM): 200 sucrose, 2.5 KCl, 1.25 NaH_2PO_4 , 10 MgSO_4 , 0.5 CaCl_2 , 26 NaHCO_3 and 11 glucose, pH 7.4, for 4–6 min. Slices were cut with a Microslicer (DTK-2000; Dosaka EM, Kyoto, Japan) in the horizontal direction with a small declining angle on the lateral side to fit the curved surface of the SC (Figs 1A and 5A). Other brain blocks were sliced in the coronal direction. These coronal slices were examined under the microscope before starting the recording experiments to confirm that the horizontal slices were properly made by observing the location and angle of the cutting edge. Horizontal slices were incubated in standard Ringer solution containing (in mM): 125 NaCl, 2.5 KCl, 1.25 NaH_2PO_4 , 10 MgSO_4 , 0.5 CaCl_2 , 26 NaHCO_3 and 11 glucose, pH 7.4, at room temperature for more than 1 h before recording.

Stimulation with the multi-electrode array

The multi-channel recording system (MED64 system; Panasonic, Japan) was employed to stimulate the slice in various locations relative to the recorded neuron. The slices were placed on the center of the MED probe, 8 \times 8 array (e.g. Fig. 1B), and perfused continuously

with standard Ringer solution at 33–34 $^\circ\text{C}$. The slices were then left for 15 min to sufficiently attach to the electrode array. Individual microelectrodes within the planar electrode array were selected by a 64-switch box and used for stimulation. Alternatively, in the two-point stimulation experiments, stimulus pulses were applied through two electrodes simultaneously. Biphasic current pulses (0.1 ms cathodal and 0.1 ms anodal) were triggered by data acquisition software (MED64 Conductor 3.1TM; Panasonic).

Stimulation with the photo-uncaging system

The photolysis reaction that releases free L-glutamate for local activation of neurons in a specific area was used to avoid passing fiber activation, which often complicates the interpretation of results obtained by electrical stimulation (Dalva & Katz, 1994). Slices were perfused with 9 mM MNI-caged L-glutamate (Tocris Bioscience, Ellisville, MO, USA), and a laser beam was emitted through a 10- μm metal pinhole and the microscope objective lens as ten 0.1-ms pulses at 1 kHz. To compare with the effect of electrical stimulation at the same distance to the recording neuron, the laser beam was directed to a location near one of the planar array stimulating points.

Application of glutamate receptor antagonist

To isolate the effects to those produced by monosynaptic GABAergic input, ionotropic glutamate receptor antagonists, 50 μM (2R)-amino-5-phosphonovaleric acid (APV) and 10 μM 6-cyano-7-nitroquinoxaline-2,3-dione (CNQX), were dissolved in the standard Ringer solution and bath applied to the recording slices 5–10 min before recording the effect of antagonists.

Recordings and analysis

Whole-cell patch clamp recordings

The procedures for whole-cell recording were described previously (Isa *et al.*, 1998; Helms *et al.*, 2004). Briefly, whole-cell patch-clamp recordings were obtained from the neurons in the SCs and SCi slices by visual control of patch pipettes. To examine the synaptic input to projection neurons, GFP-negative neurons (i.e. non-GABAergic neurons) located in the central part of the slices were selected by use of fluorescence optics, and were then clamped with patch pipettes by use of bright-field optics. For current clamp recording mode, patch pipettes were filled with a 'K-gluconate' internal solution containing (in mM): 150 K-gluconate, 2 MgCl_2 , 4 Na_2ATP , 0.3 Na_3GTP , 0.2 EGTA, 10 HEPES and 0.1 spermine, pH 7.3. By contrast, for the voltage clamp recording mode, patch pipettes were filled with a 'Cs-gluconate' internal solution containing (in mM): 120 CsOH, 10 EGTA, 2 $\text{MgCl}_2 \cdot 6\text{H}_2\text{O}$, 2 Na_2ATP , 10 Heps, 0.3 Na_3GTP and 0.1 spermine, pH 7.3. To stain the recorded neurons, biocytin (5 mg/mL; Sigma, St Louis, MO, USA) was dissolved in the solution. In all experiments, we added QX-314 (2.5 mM; Sigma) to the intracellular solution to block action potential responses. The resistance of the electrodes was 4–8 $\text{M}\Omega$ in Ringer solutions. The actual membrane potentials were corrected by the liquid junction potential of -10 mV. The neurons were recorded at their original membrane potential, -55 to -65 mV, in current clamp mode. For voltage clamp experiments, the cell membranes were clamped at either 0 mV, the reversal potential for glutamate receptor channels (i.e. excitatory postsynaptic potentials, EPSPs), or -80 mV, the reversal potential for chloride currents (i.e. inhibitory

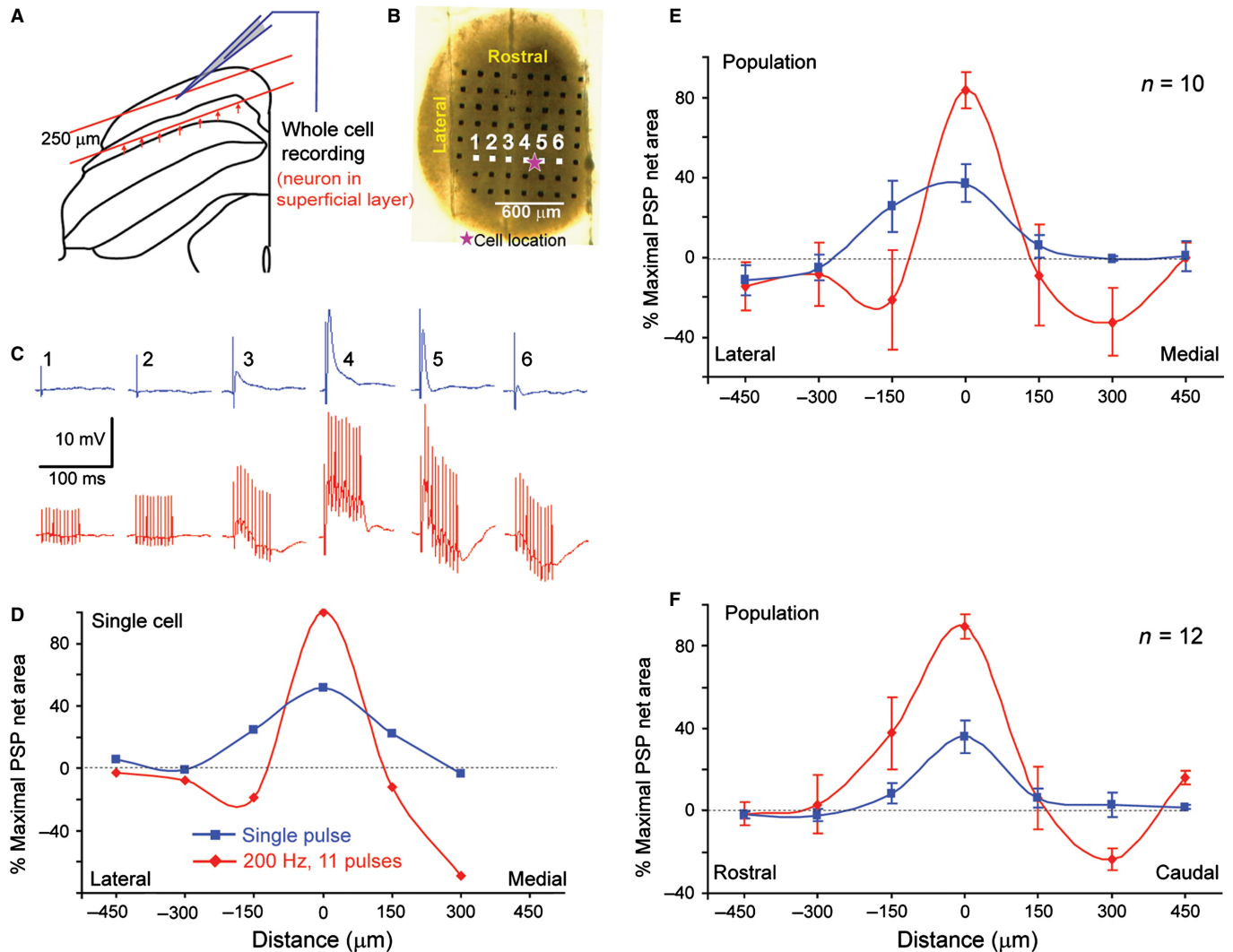


FIG. 1. (A) Schematic drawing indicating the cutting plane of the horizontal slice of superficial SC with arrangement of stimulating and recording from the coronal view. The red arrows show directions of electrical stimulation that were applied. (B) Top view of the horizontal slice of superficial SC overlying an electrode array. The pink star indicates the location of the recorded neuron. Electrical stimulation was applied from each of six electrodes in the white square while recording from the neuron. (C) The evoked EPSPs or IPSPs from the stimulation at electrodes 1–6 in B are shown for single-pulse (top row – blue traces) and 200-Hz (bottom row – red traces) stimulation. (D) The integration of EPSPs (positive value) and IPSPs (negative value) from the data in C 0–50 ms after stimulation onset is summarized and plotted on the distance axis with the closest electrode to the cell set to zero. Percentages of maximal responses were plotted against the distance between the stimulating electrode to the cell closest electrode for a single pulse (blue) and 11 pulses/200 Hz (red). (E, F) Integration of EPSPs and IPSPs from population data in the medio-lateral direction (E; $n = 10$ neurons) and the rostrocaudal direction (F; $n = 12$ neurons).

postsynaptic potentials, IPSPs). The whole cell recordings used a patch clamp amplifier (EPC-7; Heka, Lambrecht/Pfalz, Germany) connected through a Digidata1322A analog/digital interface card (Axon Instruments, Union City, CA, USA). The data were acquired using a pClamp system (pClamp 8.0; Axon Instruments).

Data analysis

Eight sweeps of intracellular responses from each stimulation protocol were averaged by using a Clampfit 10.2 software (Axon Instruments). These averaged responses were used for calculation of the integrated area under the curve using a MatLab 7.0.4 (Mathworks, Natick, MA, USA) script file. In brief, the stimulus artifacts were first detected by their sharp rise–fall characteristics and were removed. Then, the area under the curve was integrated within the desired period, 50 or 200 ms in cases of single pulse or multiple

pulses, respectively. The net areas were obtained by subtracting the negative value of the IPSP area from the positive value of the EPSP area. All data were expressed as means \pm SEM. The net area of intracellular responses to the stimulation of each electrode was transformed to the color code and mapped to locations of the corresponding electrodes (see Figs 3–6 and 8).

Results

Experiments were performed on 40 SCs slices and 34 SCi slices obtained from 39 GAD67-GFP knock-in mice (up to two SCs and two SGi slices could be obtained from each animal). Whole cell patch clamp recordings were obtained from 51 neurons in the SCs and 46 neurons in the SCi, all of which were identified as non-GABAergic neurons due to the absence of GFP fluorescence in the genetically altered mice. Stimulus strength from each electrode was

fixed for each neuron at the current intensity which gave maximal responses (normally 120–180 μ A), if not noted.

Excitatory and inhibitory lateral interactions in the SCs

The horizontal slices of the SCs were placed on the array of micro-electrodes. The deeper part of the optic layer (stratum opticum, SO) was positioned toward the planar electrodes (red arrows in Fig. 1A) so that retinal axons supplying SCs were adjacent to the electrode array, optimizing stimulation. The effects of electrical stimulation through the electrode array are illustrated for one neuron (pink asterisk, Fig. 1B), as the stimulation site was varied systematically along the medio-lateral axis across six adjacent stimulating electrodes (Fig. 1C). Stimulation with the electrode immediately lateral to the neuron (i.e. location #4) evoked EPSPs in response to a single pulse (Fig. 1C, top row). This excitatory effect was more prominent with the increased stimulus frequency and number of pulses (Fig. 1C, bottom row). Stimulation further laterally (location #3) produced a smaller depolarization (Fig. 1C, top row) that was followed by a longer latency IPSP when multiple stimuli were used (Fig. 1C, bottom row). More lateral stimulation (locations #1 and #2) produced no effect. Stimulation at a site immediately medial to the recorded neuron (location #5) produced an EPSP (Fig. 1C, upper row). A train of stimuli resulted in an EPSP–IPSP sequence (Fig. 1C, lower row). Stimulation further medially (location #6) produced just the hyperpolarization following a train of stimuli (Fig. 1C, lower row).

We quantified the evoked responses as a function of distance between stimulation and recording locations with two different stimulus protocols, single pulse vs. multiple pulses (11 pulses, 200 Hz, for 50 ms). As shown in Fig. 1D, the excitatory effect was strong when the site of stimulation was close to the neuron recorded. The excitatory effect in the illustrated cell was found within a radius of approximately 100–150 μ m. This ‘excitatory area’ was surrounded by an area from which inhibition was induced. There was considerable cell-to-cell variation in the response pattern, and as shown in Fig. 1E, we calculated the average normalized amplitude of net excitation and inhibition from ten superficial layer neurons from medio-laterally arranged stimulating electrode arrays. The responses were symmetrical along the medio-lateral direction, but they were not symmetrical along the rostral-caudal direction (Fig. 1F). From the population averages, inhibition was found only on the caudal side, whereas the net population effect was excitatory on the rostral side. This was because, in some neurons, only excitation was induced from stimulation sites rostral to the recorded neurons. We presumed that this asymmetrical shape might be caused by the complication of rostral site stimulation, which might additionally activate afferent fibers of passage, mostly retinotectal fibers that enter the SC from the rostral side and project caudally through the SO layer (Godement *et al.*, 1984).

To avoid activating fibers of passage, we also examined the effect of photo-stimulation leading to uncaging of free glutamate (Dalva & Katz, 1994). Although electrical stimulation of the rostral site induced excitation in the cell shown in Fig. 2, photo-stimulation induced inhibition from electrode locations on both rostral and caudal sides to the cell. The result was supported in additional experiments ($n = 4$, Fig. 2D). Thus, as long as we could avoid electrical stimulation of passing fibers, center excitation and surround inhibition was the most commonly observed input organization to the SCs neurons.

We analysed the full spatio-temporal profile of the EPSPs and IPSPs. Figure 3B illustrates the profiles evoked in a single superficial layer neuron (pink asterisk in Fig. 3A) by stimulation at various

locations across the SC map. The excitatory and inhibitory responses had different spatial and temporal profiles during the 50-ms train of repetitive pulses. Excitation was elicited shortly after the first stimulus pulse when stimulation was applied adjacent to the cell, whereas the inhibition built up more gradually for stimulation at remote locations (Fig. 3B). Thus, both excitatory and inhibitory areas expanded during application of train stimuli, indicating that repetitive stimuli recruited a larger number of neurons, particularly from remote sites, compared with a single stimulus. The inhibitory input reached its maximal amplitude at the end of stimulation (i.e. 50 ms after the first stimulus; Fig. 3C). In contrast, the excitatory input peaked before 10 ms and was considerably weaker ($> 50\%$) at the end of the train (Fig. 3C and D). The latencies of the excitatory input of the SCs neurons were 2.38 ± 0.41 ms ($n = 19$), which suggested that the earliest component was of monosynaptic origin. Inhibitory signals were obtained following stimulation of more distant regions, conveyed by either the long horizontal projections or through polysynaptic connections that arrived at longer latency (7.79 ± 0.90 ms, $n = 19$; significantly longer than the excitation, paired Student’s *t*-test, $P = 0.0016$). Figure 3C and D show the time course of EPSPs and IPSPs at a single cell and population levels, respectively. It was thus confirmed that excitation first increased and then inhibition followed. The results were also confirmed in voltage clamp recordings described below (Figs 4 and 7).

Isolating excitatory and inhibitory inputs in SCs neurons

The presence of both excitatory and inhibitory responses suggests that looking at the sum of excitation and inhibition is not the best means to determine the full range of possible connections. For example, short-range inhibitory connections could be masked by excitation, which was earlier to develop and could also be more dominant (Figs 2 and 3). Because of this possible overlap, it was necessary to explore excitatory and inhibitory signals to the SCs neurons independently. Voltage clamp recording at two different holding potentials enabled us to examine this point. Excitatory postsynaptic currents (EPSCs) were tracked exclusively at -80 mV, the equilibrium potential of chloride ions that pass through the GABA_A receptor channels. Inhibitory postsynaptic currents (IPSCs) were observed exclusively at 0 mV, the equilibrium potential of ionotropic glutamate receptors. The reversal of each synaptic current component at the above membrane potential with the present extracellular and intracellular solutions was confirmed in separate experiments (data not shown).

Figure 4B shows the results of repetitive stimulation applied across the SC while recording from a single SCs neuron clamped at -80 mV (top row of traces) and 0 mV (bottom row), to respectively investigate the profiles of EPSCs and IPSCs in isolation. The color images in Fig. 4C show the integrated area of EPSCs (top row) and IPSCs (bottom row) for each 10-ms period during the initial 50 ms of repetitive stimulation. Both excitatory and inhibitory responses reached the maximum amplitude during the period of 0–20 ms (time to peak, 6.12 ± 1.56 ms for EPSC, and 13.23 ± 1.92 ms for IPSC, $n = 24$ significantly different $t = -2.7569$, d.f. = 23, $P = 0.0112$, paired *t*-test) after stimulation onset and then declined gradually. However, their temporal profiles were different (see below); the excitation decreased earlier than inhibition. As a result, the area of the excitatory input field became smaller than that of the inhibitory input field during the periods 30–40 and 40–50 ms. Figure 4D shows the normalized 10-ms integrated areas of EPSCs and IPSCs for a group of nine SCs neurons, plotted on the distance axis in the medio-lateral direction across the maximal response. Although not significantly different ($t = -2.8037$, d.f. = 3, $P = 0.1072$, paired *t*-test), the plots

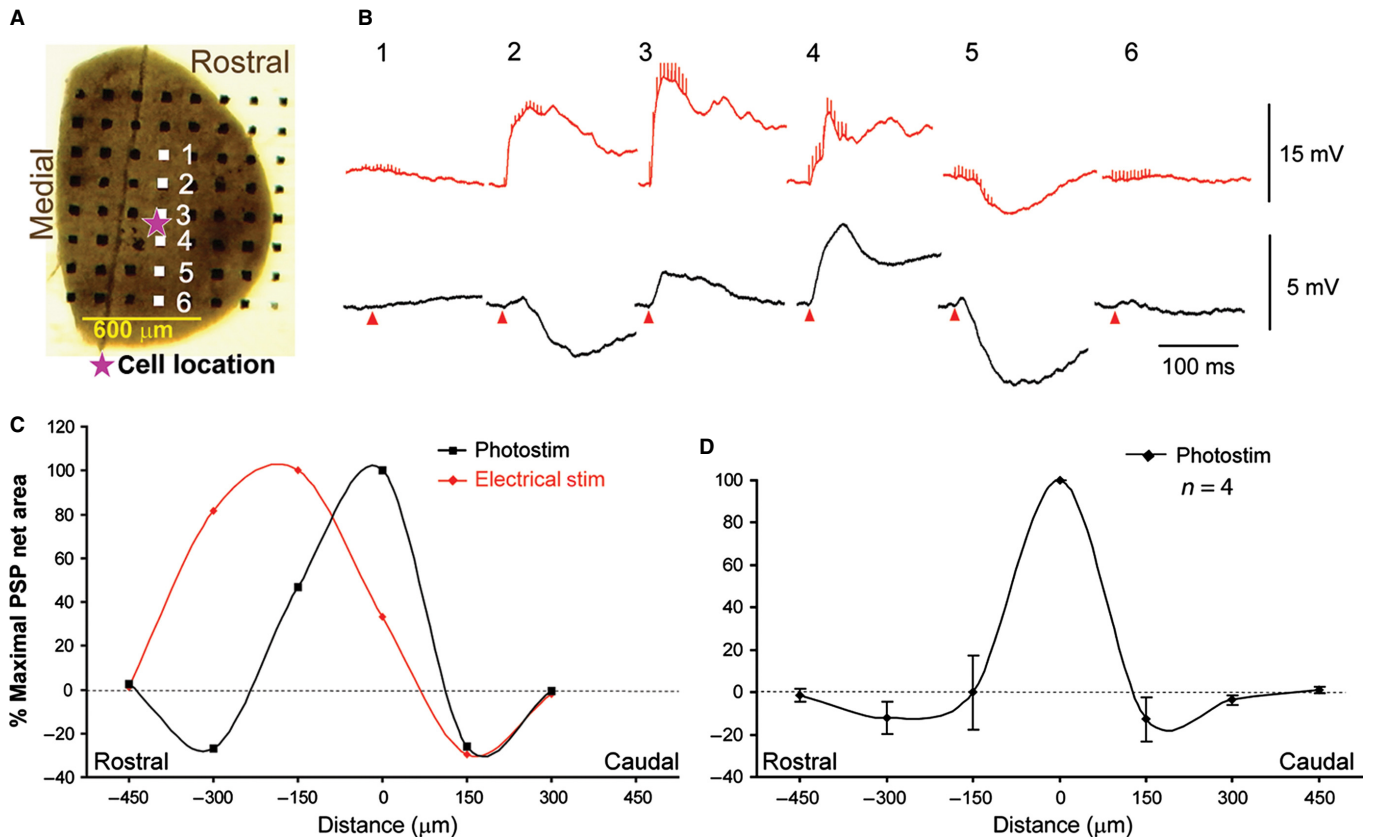


FIG. 2. Effects of photo-stimulation with caged glutamate in SCs. (A) The horizontal slice overlying an electrode array indicating the stimulating electrode (white square) and the site of recording neuron (pink star). (B) EPSPs or IPSPs evoked by the electrical stimulation at electrode positions 1–6 are shown in the top row (red), and the EPSPs or IPSPs evoked by the photo-stimulation at the same slice locations as the electrical stimulation are shown in the bottom row (black). Red arrowheads indicate photo-stimulation start time. (C) Percentage of maximal responses from the data in B plotted against the distance between the stimulating electrode to the cell closest to the electrode in the rostrocaudal direction, comparing between two types of stimulation systems, electrical stimulation (red) and photo-stimulation (black). (D) Percentage of normalized maximal responses evoked by photo-stimulation in the population ($n = 4$ neurons).

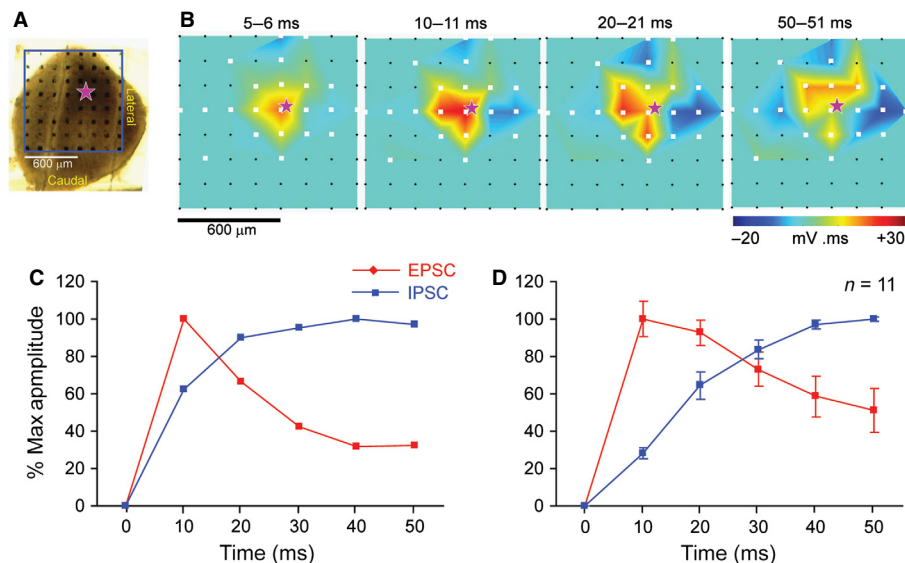


FIG. 3. (A, B) One-millisecond integrated areas of EPSPs or IPSPs evoked in an SCs neuron at the pink star (in A) at different times after the stimulus were computed and indicated in colors: positive values are red and negative values are blue. They are mapped on the location of each stimulating electrode. Only electrodes marked with white squares were tested. (C) The time course of excitation and inhibition recorded over 11 superficial layer neurons. (D) Population data of the time course of excitation and inhibition recorded over 11 superficial layer neurons.

indicated that the IPSC areas tended to be broader than the EPSC areas (the half-width area, EPSC = $129.822 \pm 10.387 \mu\text{m}^2$, IPSC = $145.632 \pm 15.192 \mu\text{m}^2$, $n = 4$), particularly during the later

epoch (40–50 ms after stimulation onset). This finding was confirmed within a similar experimental protocol that used the laser uncaging system to stimulate the SCs (Fig. 4E).

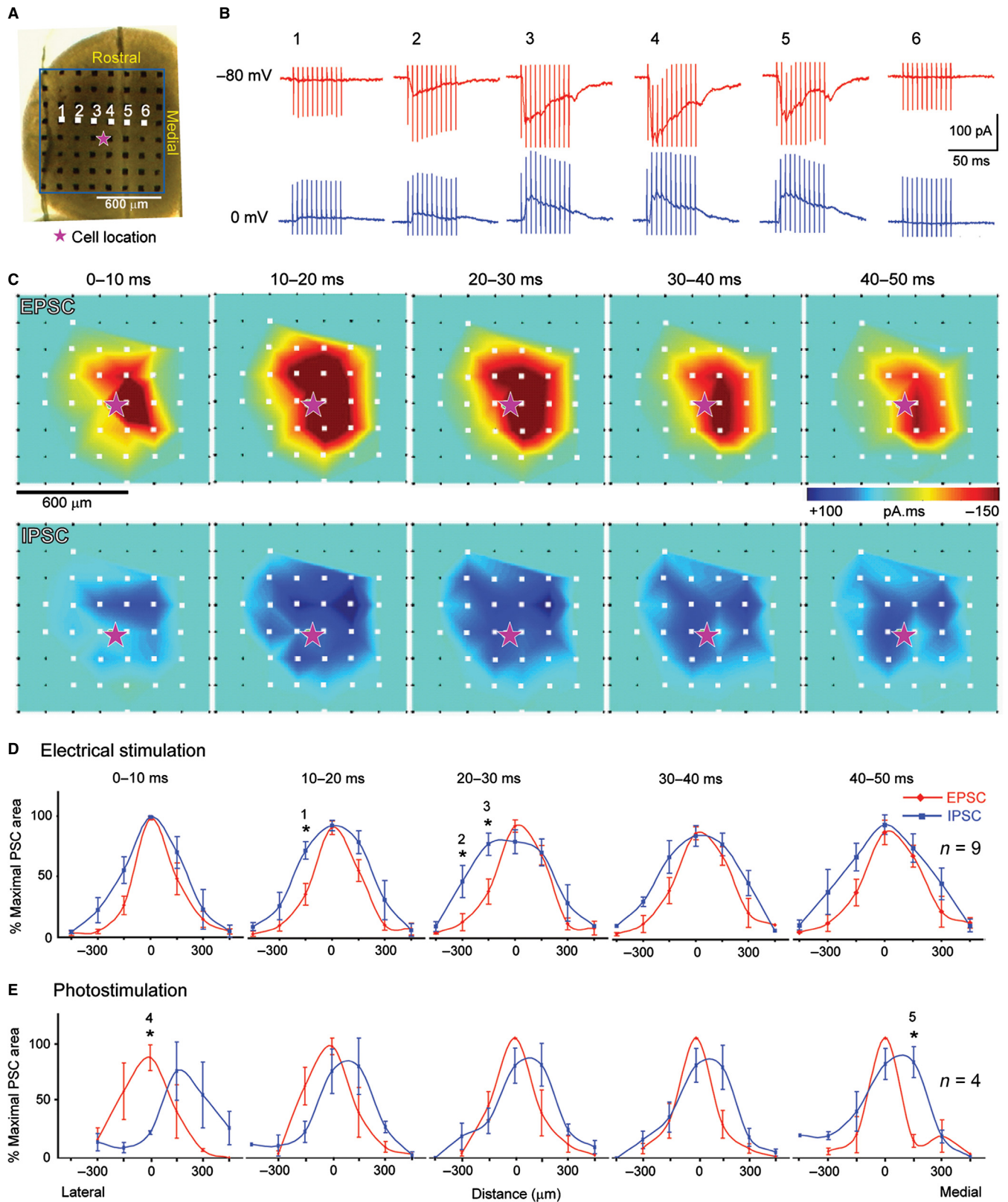


FIG. 4. (A) Horizontal slice overlying an electrode array showing the location of the recorded neuron. (B) Whole cell voltage clamp recording from a SCs neuron with two different holding potentials, -80 mV (top row) and 0 mV (bottom row). (C) Ten-millisecond integrated area of EPSCs or IPSCs computed to red and blue colors, respectively, and mapped to the location of each stimulating electrode. The 200-Hz stimuli were applied for 50 ms. Only electrodes marked with white squares were tested. (D, E) Percentage of maximal responses of postsynaptic current (PSP) integrated in each 10 ms after stimulation from 0 to 50 ms plotted on distance between the stimulating electrode to the cell closest to the electrode in the medio-lateral direction. The responses evoked by electrical stimulation and photo-stimulation are shown in D ($n = 7$) and E ($n = 4$), respectively. An asterisk (*) indicates statistically significant differences (unpaired Student's *t*-test, $P < 0.05$). Numbers 1–5 with asterisks indicate each point that showed a significant difference between the EPSCs and IPSCs.

Excitatory and inhibitory lateral interactions in the SCi

We also investigated lateral connectivity across the SCi by making slices mainly comprising the SCi and placing them upside down on the electrode array (Fig. 5A) so that stimulation was delivered to the SO layer side of the slice through which many inputs arrive in SCi either from the SCs or via collaterals of axons innervating the SCs originating either from the visual cortex or the SCi (Lee *et al.*, 1997; Isa *et al.*, 1998; Helms *et al.*, 2004; Phongphanphane *et al.*, 2008). Most SCi neurons were recorded close to the top of the slice (i.e. ventral part of the SCi) and the effect of electrical stimulation of the SO (dorsal-most aspect) was tested. Both single-pulse and repetitive stimulation across the medio-lateral extent of the SC predominantly induced excitation, as shown by the neuron illustrated in Fig. 5C. Single-pulse stimulation induced EPSPs from nearby electrodes and repetitive stimulation induced excitation from more distant sites for the sample neuron (Fig. 5D). The population profile ($n = 8$) of the excitation was symmetrical in both the medio-lateral

and the rostral-caudal directions for the group of SCi neurons sampled (Fig. 5E and F, respectively).

We also employed the uncaging of glutamate to ensure that the responses recorded from SCi neurons were not primarily due to activation of axons of passage. The responses evoked by the uncaging of glutamate (Fig. 5G) demonstrated similar spatial properties. As shown in the two-dimensional color plots in Fig. 5I, the excitation in the SCi appeared to grow gradually during the stimulation period and only declined after the stimulation was terminated. This was different from in the SCs, in which the peak response appeared during a relatively early period of the stimulation (Fig. 3).

Isolating excitatory and inhibitory inputs in the SCi neurons

To determine whether inhibition was really absent in the SCi, or instead masked by the widespread excitation, we performed voltage clamp experiments to isolate excitation and inhibition. In addition to the EPSCs revealed at -80 mV (Fig. 6B, top), we also observed

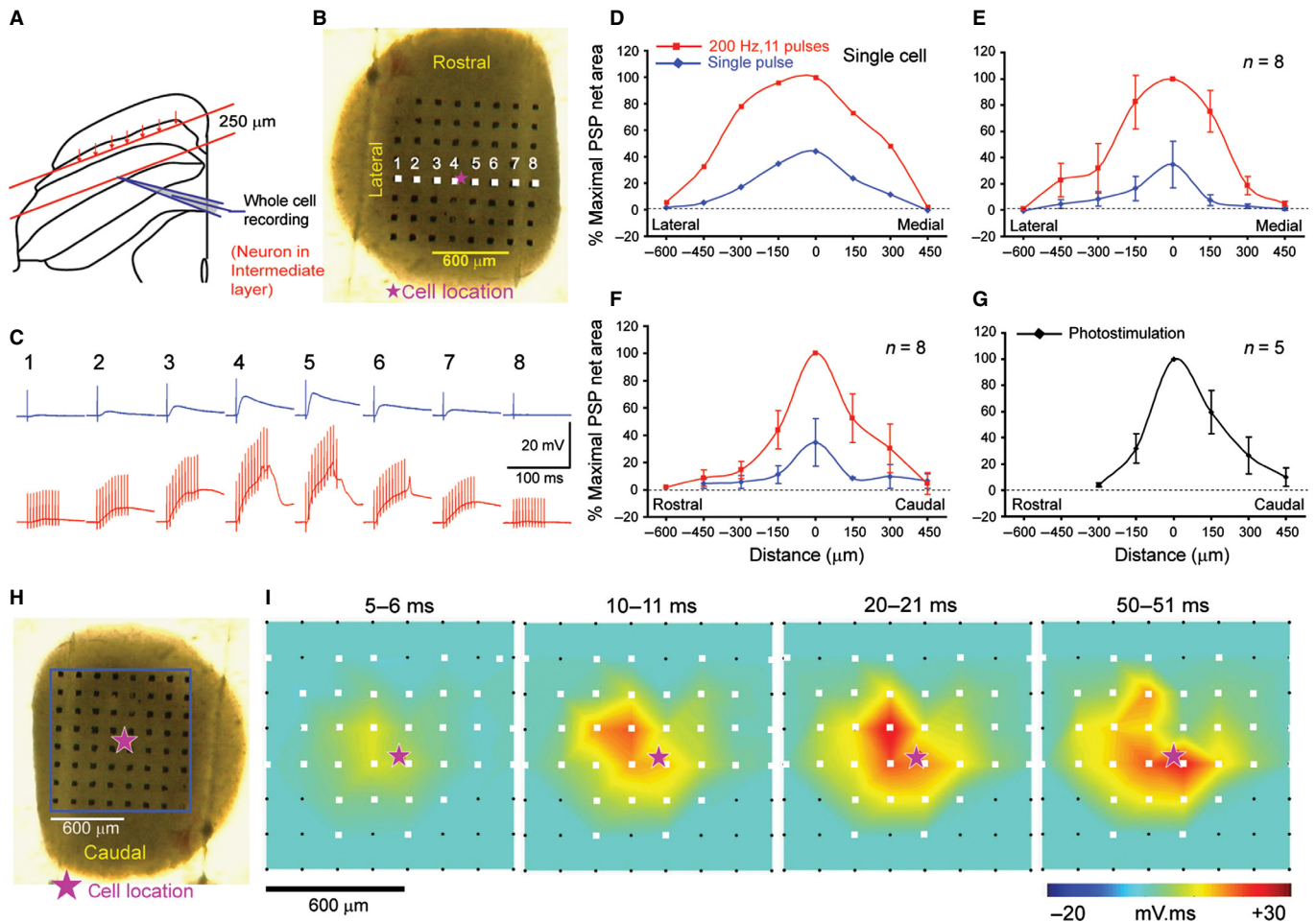


FIG. 5. Recording from the SCi. (A) Schematic drawing indicating the cutting plane of the horizontal slice and this arrangement of stimulating and recording system in coronal view. The intermediate layer slices were placed upside-down on the dish with the electrode array shown by the small red arrows. (B) The upside-down horizontal slice overlying an electrode array. The pink asterisk indicates the location of a recorded SCi neuron. The electrical stimulation to the cell was applied from each of eight electrodes in the white squares. (C) The evoked EPSPs or IPSPs from the stimulation from electrodes 1–8 in B are shown in two rows of different stimulus protocol, namely single pulse (blue) and 11 pulses at 200 Hz (red). (D) Integration of EPSPs and IPSPs during 0–50 ms after starting stimulation summarized and plotted on the distance axis, such that the closest electrode to the cell was set to zero. (E, F) Percentage of maximal responses plotted against the distance between the stimulating electrode and the cell closest to the electrode in two directions, rostrocaudal (E, $n = 8$) and medio-lateral (F, $n = 8$). Two stimulus protocols were tested, namely single pulse (blue) and 11 pulses/200 Hz (red). (G) Percentage of maximal responses evoked by the uncaging photo-stimulation plotted against the distance in the medio-lateral direction ($n = 5$). (H) The intermediate layer slice overlying an electrode array. (I) One-millisecond integrated areas of EPSPs or IPSPs evoked in the SCi neuron were converted to colors, and mapped to the location of each stimulating electrode (format as in Fig. 3B).

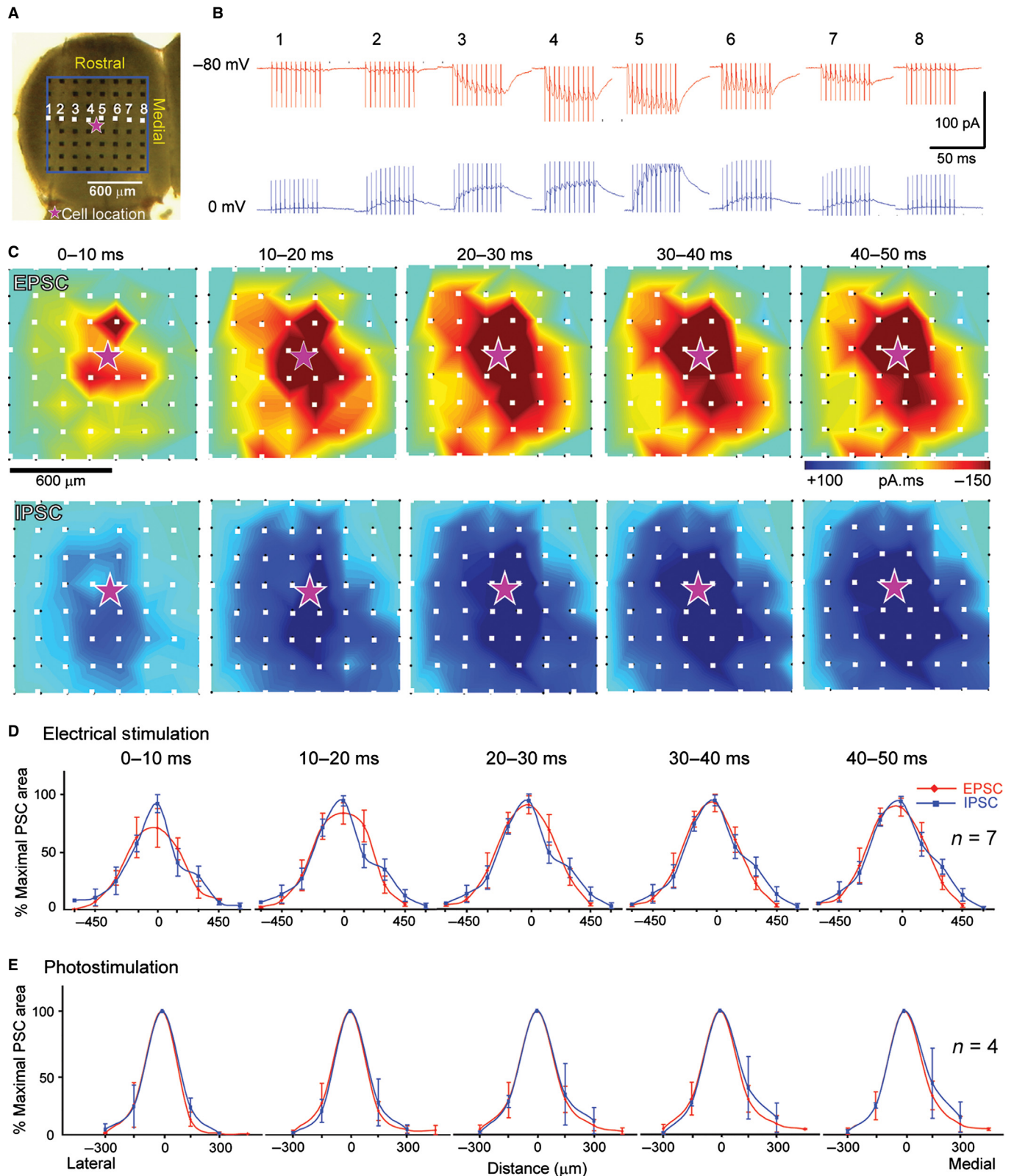


FIG. 6. Dissociation of EPSCs and IPSCs in SCi neurons. (A) The horizontal slice overlying an electrode array. (B) Whole cell voltage clamp recording was performed in SCi neurons at two different holding potentials, -80 mV (top row, red) and 0 mV (bottom row, blue). (C) Ten-millisecond integrated areas of EPSCs or IPSCs were converted to red and blue colors, respectively, and mapped on the location of each stimulating electrode. The 200 -Hz stimulus was applied for 50 ms. Only electrodes marked with white squares were tested. (D) Percentage of maximal postsynaptic current (PSC) integrated in each 10 ms after stimulation from 0 to 50 ms plotted against the distance between the stimulating electrode and the cell closest to the electrode in the medio-lateral direction ($n = 7$). (E) Percentage of maximal responses evoked by the uncaging photo-stimulation plotted against the distance in the medio-lateral direction ($n = 4$).

clear IPSCs by clamping the membrane potential at 0 mV (Fig. 6B, bottom). As shown in the two-dimensional color plots (Fig. 6C), the area from which EPSCs and IPSCs were induced mostly overlapped. The population data of integrated EPSC and IPSC area evoked by either electrical stimulation (Fig. 6D) or photo-stimulation (Fig. 6E) revealed similar spatial and temporal profiles for both excitatory and inhibitory responses. Therefore, the lack of inhibitory responses in the SCi was largely due to masking by more dominant excitation.

Temporal profiles of synaptic transmission in the SCs vs. SCi

Figure 7A shows the normalized temporal profiles of excitation and inhibition induced by repetitive stimulation in SCs and SCi neurons. Both excitatory and inhibitory processes decreased during repetitive stimulation in all of the SCs neurons recorded ($n = 10$). The time constants for the desensitizing phase were 49.4 ± 3.9 and 84.0 ± 10.2 ms for excitation and inhibition, respectively (Fig. 7B, left) (significant difference, unpaired Student's *t*-test, $P = 0.0042$). Thus, the declining phase was slower for inhibition. These results may account for the different spatio-temporal profiles of excitation and inhibition (Fig. 3F and G). In contrast, the SCi neurons ($n = 10$) showed increasing synaptic properties for both excitation and inhibition during repetitive stimulation. The time constants of the rising phase were 7.3 ± 2.2 and 9.5 ± 1.1 ms for excitation and inhibition, respectively (Fig. 7B, right) (unpaired Student's *t*-test, $P = 0.4022$, n.s.). These differences in temporal properties of excitation and inhibition might be reflected in the different structure of excitation and inhibition fields in SCs (Fig. 4C) and SCi (Fig. 6C) neurons. Such differences in the synaptic properties probably represent the functions of the local circuits of the individual layers. The SCs might be better suited for detecting the change of the inputs, while the SCi might be better suited for accumulating or integrating the input signals to produce presaccadic burst activity to generate saccadic eye movements in the downstream brainstem circuits (Boehnke & Munoz, 2008). In SCs neurons, in particular, although both EPSC and IPSC amplitude decreased during repetitive stimulation, the EPSCs decayed significantly faster than the IPSCs and this might contribute to the enhanced inhibitory response that emerged after the initial excitation.

Long-range monosynaptic inhibition in SCs and SCi

Lateral inhibitory interactions were identified in both SCs and SCi (Figs 3 and 5), as neurons were inhibited by distant electrode stimulation. However, these lateral inhibitory connections could be the result of either direct activation of remote GABAergic neurons, or indirect activation of local inhibitory interneurons via excitatory synapses from glutamatergic neurons with long horizontal axons. To clarify the extent of the direct horizontal inhibition in both layers, we applied glutamate receptor antagonists ($10 \mu\text{M}$ CNQX and $50 \mu\text{M}$ APV) to remove the polysynaptic excitatory components. Voltage clamp recording was performed in both SCs (Fig. 8A) and SCi (Fig. 8B) with the holding potential at 0 mV to demonstrate only the inhibitory response. The color plot shows the averaged responses in 10-ms time bins during repetitive stimulation ($60\text{--}180 \mu\text{A}$, 200 Hz, 11 pulses). Application of the antagonists explicitly reduced the inhibitory response in both SCs and SCi. Among neurons in the SCs ($n = 6$), removal of the polysynaptic components produced a marked reduction in the extent of the propagation of inhibition. The half width of the extent of the direct inhibition was $302 \mu\text{m}$ and 90% range was $429 \mu\text{m}$ in SCs neurons (Fig. 8C, left). By contrast, removal of glutamatergic polysynaptic components in the SCi reduced the amplitude,

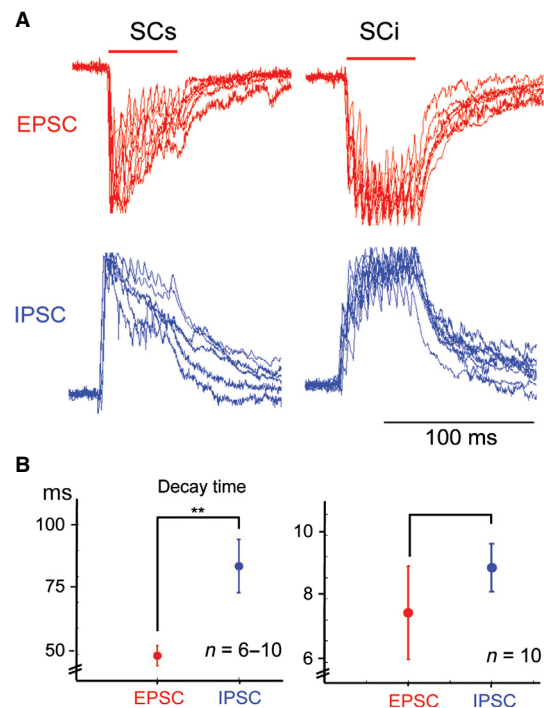


FIG. 7. Contrast between the time course of excitatory and inhibitory responses in the superficial and intermediate SC. (A) After removal of stimulus artifacts, the normalized EPSCs (red) and IPSCs (blue) evoked by the closest stimulating electrode are plotted in two columns, superficial slices and intermediate slices, respectively ($n = 6\text{--}10$). The red bars on the top indicate the duration of repetitive stimulation. (B) Left: the decay time constant of EPSCs and IPSCs in superficial layer neurons (mean and SE). Right: rising time constant of EPSCs and IPSCs in intermediate layer neurons (mean and SE). ** $P < 0.01$.

but not so much the extent of lateral inhibition (Fig. 8B). The half width of the extent of direct inhibition was $521 \mu\text{m}$ and 90% range was $\geq 900 \mu\text{m}$ in SCi neurons ($n = 4$) (Fig. 8C, right).

The interaction of two-point stimulation

It is well known that in behaving monkeys, a distractor presented close to a saccade target causes vector averaging of neural activity, which results in saccades directed to the location between the target and distractor, while a distractor presented remotely relative to the target attenuates the visual responses to the target (Edelman & Keller, 1998; Dorris *et al.*, 2007). To mimic such target-distractor interactions and explore the local circuit mechanisms which could explain such observations, we applied electrical pulses to two stimulating electrodes simultaneously and systematically varied their distance from the recorded neuron. One stimulation site was located very close to the recorded neuron, while another was placed various distances away from the cell. Representative raw data of current clamp recordings from an SCs neuron are shown in Fig. 9B; the responses evoked by single-point repetitive stimulation are in the upper row and the two-point repetitive stimulation in the lower row. As shown for a single neuron (Fig. 9C) and the population of neurons tested (Fig. 9D, $n = 8$), the response net area of the two-point stimulation at the $150\text{-}\mu\text{m}$ location was substantially higher than the linear summation of responses evoked by two single stimuli alone. The interaction depended on the balance of intensities of the two stimuli. In the case shown in Fig. 9E, two points separated by $450 \mu\text{m}$ were stimulated. As shown in the upper row, stimulation of point 1 (close to the

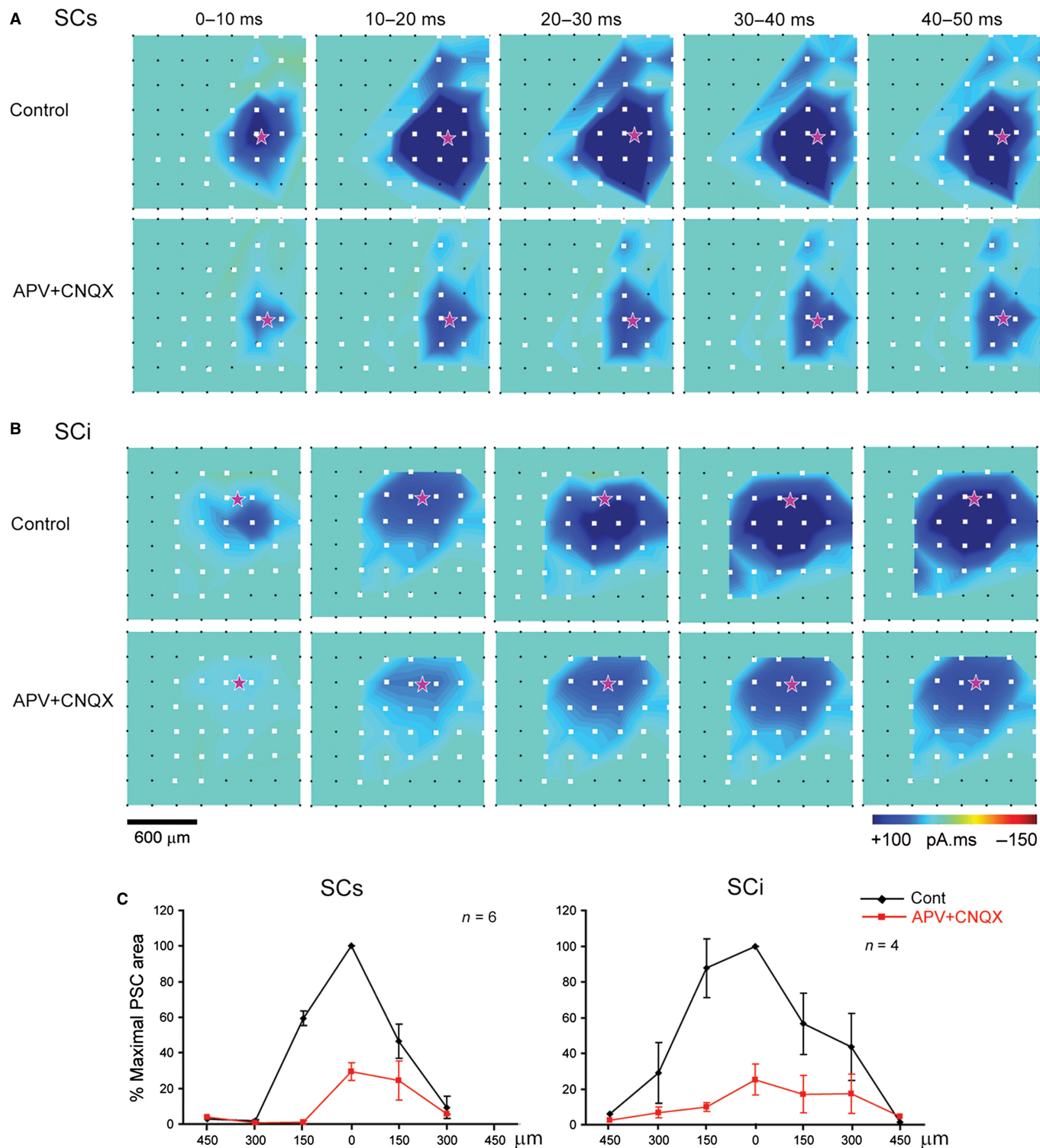


FIG. 8. Effects of suppressing the glutamate receptor-mediated synaptic transmission on the lateral inhibitory interaction in the SCs and SCi. The membrane potential of the recorded cells was voltage-clamped at 0 mV to eliminate the EPSCs. (A) An example of an SCs neuron. Average IPSCs are indicated for different time period following the stimulation. Upper: control. Lower: following administration of 50 μM APV and 10 μM CNQX. (B) Example of an SCi neuron. The same arrangements as A. (C) Population data for the SCs ($n = 6$, left) and SCi ($n = 4$, right) neurons. Black lines indicate the control data and red line the data after administration of APV and CNQX.

recorded neuron) induced mainly EPSPs and stimulation of point 2 at 120 μA induced maximal IPSPs in the cell recorded close to point 1. When the stimulation of point 1 was much stronger (180 μA in this case, which evoked maximal excitatory response), simultaneous

stimulation of points 1 and 2 induced the EPSPs with similar amplitude as that induced by stimulation of point 1 only. Thus, the effect of inhibition by stimulation of point 2 was completely eliminated. In contrast, as shown in the lower panel, when point 1 was stimulated

with relatively weak current intensity (90 μA), the EPSPs induced by point 1 were substantially knocked down when stimulated simultaneously with point 2 (at 120 μA). Thus, we fixed the stimulation intensity of the distant electrode to induce the maximal IPSPs and varied the stimulus intensity of the close point that gives maximal responses (120–180 μA) or relatively weaker current (30–120 μA) (Fig. 9F). Then, when one stimulation site was much stronger than the other, the two-point stimulation exhibited a winner-take-all-like interaction. Quantitative measurement in this case is shown in Fig. 9F. These experiments were conducted on six SCs neurons and the result was consistent (Fig. 9G).

Two-point stimulation in the SCi produced different effects. For the individual cell shown in Fig. 10A–C, stimulation of point 3 (close to the cell) induced the greatest excitation, while stimulation of points 2–5 induced weaker excitation and stimulation of point 1 induced no excitation (the upper row in Fig. 10B and violet lines in Fig. 10C). As shown in the lower panel in the bottom row in Fig. 10B and red lines in Fig. 10C, simultaneous stimulation induced effects similar to algebraic summation. This result was confirmed in the population data ($n = 8$) as shown in Fig. 10D.

Discussion

It is well known that the SCs and SCi are organized into retinotopically coded visual and saccadic motor maps, respectively (Sparks, 1986). To understand the fundamental structure of these maps, it is necessary to analyse the spatial properties of signal processing. The spread of activation along the dorso-ventral axis in the coronal plane has been studied by analysing the local field potentials with a multi-channel electrode array (Phongphanphane *et al.*, 2008) or by using voltage-sensitive dye imaging (Vokoun *et al.*, 2010, 2011). However, until now, the full extent of the lateral interactions within the same layer has not been studied. In this study, we have introduced a new *in vitro* experimental system, horizontal SC slices, in which the lateral connections within the SCs and SCi were preserved. In these preparations, stimulation, either by electrical or by photochemical means, was applied to various locations across the collicular map, while whole-cell recordings were made from single neurons.

We examined the lateral interactions within the SCs and SCi in isolation. In the SCs slices, the afferent input fibers to the cells close to the stimulating electrodes were presumed to be activated by the electrodes attached to the ventral side of the slices. These afferent fibers may include the retino-tectal fibers, which are known to innervate a relatively confined area of the SCs (Tamamaki *et al.*, 1995). Cortico-tectal fibers and those originating from SCi and projecting to SCs may have also been stimulated. The latter axons were originally shown to be mainly inhibitory (Lee *et al.* 2007), although a recent study showed some of them might be excitatory (Vokoun *et al.*, 2010, 2011). Axons of the SCs neurons projecting toward SCi may have been antidromically stimulated, but the antidromic spike would have been eliminated by QX-314 contained in the intra-pipette solution, but the synaptic effects mediated by their collaterals cannot be excluded.

In the SCi slices, the stimulation applied to the dorsal side of the slices probably activated the axons either from the SCs or via collateral axons innervating the SCs originating from either visual cortex or SCi. However, in both SCs and SCi slices, we observed similar responses by using electrical and photo-uncaging stimuli, with one exception; when the rostral SC was stimulated electrically, activation of optic fibers running from the rostral to caudal direction was a likely contaminant (see Fig. 2). Otherwise, the results from both electrical and chemical stimulation could be ascribed to the

activation of the neural elements originated from around the stimulation sites. This suggests strongly that the present results of electrical stimulation closely mimicked the effect caused by physiological activation of the cell population close to the stimulation site. Stimulation of passing fibers that do not innervate the neurons near the electrode can therefore largely be neglected.

We demonstrated that both the SCs and the SCi contain lateral excitatory and inhibitory connections that are extensive and overlapping. There were, however, important differences between SCs and SCi with regard to their spatial and temporal profiles of the lateral interactions, as will be discussed below. These results suggest strongly that the two layers employ different signal processing machinery.

We initially intended to correlate the somato-dendritic morphology of the recorded cells and the effect of electrical stimulation from individual electrodes. However, it was not easy to make clear classification even between the narrow-field vertical cells and wide-field vertical cells in the horizontal SCs slices, because the ratio of tissue shrinkage during preparation of histology was different along the horizontal and dorsoventral axes of the slices. Moreover, it was not easy to correlate the dendritic morphology and synaptic effects from individual electrodes. This was because the synaptic effects appeared to include polysynaptic components, and the inter-electrode interval (150 μm) was too long to make precise estimations. We concluded that for this purpose, the electrode array will require shorter inter-electrode distances or mapping with a laser uncaging technique. We therefore abandoned this analysis in this study.

Lateral interactions in the SCs

Both lateral excitation and inhibition were found over a wide range in the SCs (Fig. 4). However, inhibition dominated excitation, and a Mexican-hat-like, center excitation-surround inhibition type of lateral interaction was observed. Relatively strong inhibition in the SCs might be partly due to its higher density of GABAergic interneurons (Mize, 1992). The spatial relationship of excitation and inhibition in the SCs is summarized in Fig. 11 (left). After removal of excitatory synaptic transmission (Fig. 8A and C), the extent of lateral inhibition became shorter, but lateral inhibition was still observed within a distance of 150–200 μm . Such lateral inhibition is probably mediated by a group of horizontal cells with long dendritic arborizations (Endo *et al.*, 2003). The marked shrinkage of the lateral inhibition in Fig. 8A and C might have been caused by difficulty in directly activating the horizontal cells, which are most densely distributed close to the dorsal surface of the SC (Langer & Lund, 1974) by stimulation through the electrodes attached to the SO side of the slices.

When two different sites in the SCs were stimulated, sites in close proximity markedly facilitated the excitation in a non-linear fashion, while stimulation of remote sites markedly inhibited the excitation induced by stimulation of a close point. The remote inhibition could even knock down the excitation when stimulation was relatively strong for the remote site (Fig. 9E, lower). These contrasting effects between stimulation of close and remote sites suggest that the lateral interactions in the SCs are suitable for enhancing the spatial contrast of visual stimuli.

As shown in Fig. 7, when repetitive stimulation was applied, both lateral excitation and inhibition sharply decreased in the SCs. Excitation decreased faster than inhibition. This was a common finding over all the recorded SCs neurons. This result suggests that synapses in the SCs are optimized for detecting spatiotemporal changes in visual stimuli.

Thus, both the spatial and the temporal profiles of lateral interactions in the SCs suggest that the local circuits of the SCs are

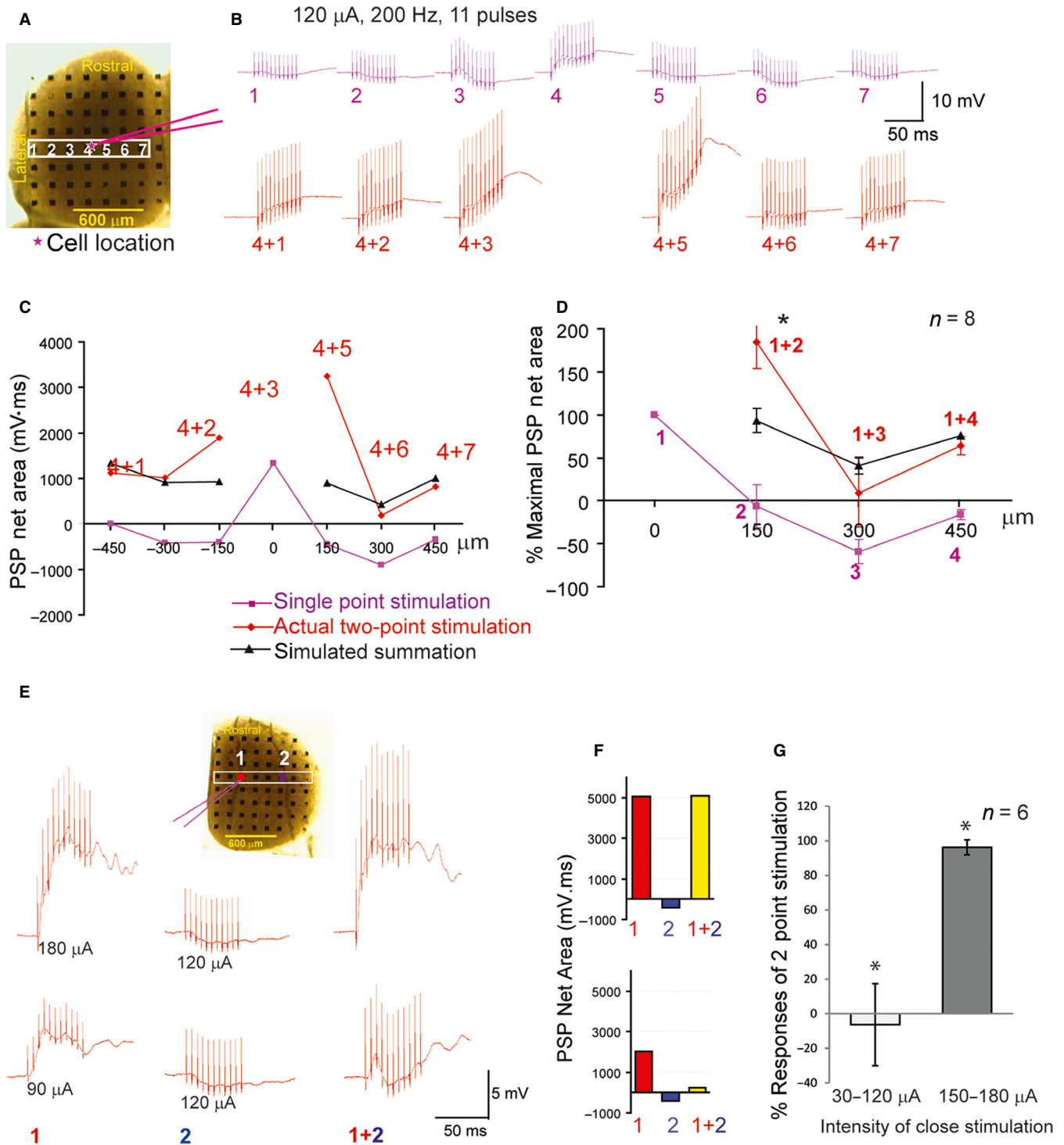


FIG. 9. Effects of simultaneous stimulation of two points on SCs neurons. (A) Arrangement of stimulation electrodes. The location of the example neuron from which the whole cell recording was made is indicated by a pink asterisk. It was close to electrode #4. (B) The effects of single point stimulation (upper panels in violet) and two-point stimulation (lower panels in red). (C) PSP net area for the data shown in B, plotted against the horizontal distance from the recording site. Violet lines indicate the effect of single-point stimulation (upper row in B). Red lines indicate the actual data from two-point stimulation. Black lines indicate the algebraic summation. (D) Population data from eight SCs neurons, plotted against horizontal distance, neglecting the medio-lateral polarity. As in C, the violet line indicates the data of the single electrode stimulation, the red line indicates the actual data of the two-point stimulation, and the black line indicates the algebraic sum. *Significant difference from the algebraic sum ($P < 0.05$). (E) Winner-takes-all-like interaction between the two points. Recording was made from the cell near electrode 1. Stimulation was applied at points 1 and 2 in the inset. In the upper row, the effect of stimulating point 1 at 180 μ A (left), the effect of stimulating point 2 at 120 μ A (middle), and the effects of simultaneous stimulation (right) are indicated. In the lower panel, the effects of stimulating point 1 at 90 μ A (left), the effect of stimulating point 2 at 120 μ A (middle), and the effects of simultaneous stimulation (right) are indicated. (F) PSP net area for the records shown in E. (G) Population data of changing the balance of two-point stimulations ($n = 6$ cells). When a nearby point was stimulated at relatively weak levels, the double stimulation resulted in almost complete suppression of the excitation (left), while if the nearby point was stimulated at higher intensity, virtually no inhibition was observed (right) ($P < 0.005$).

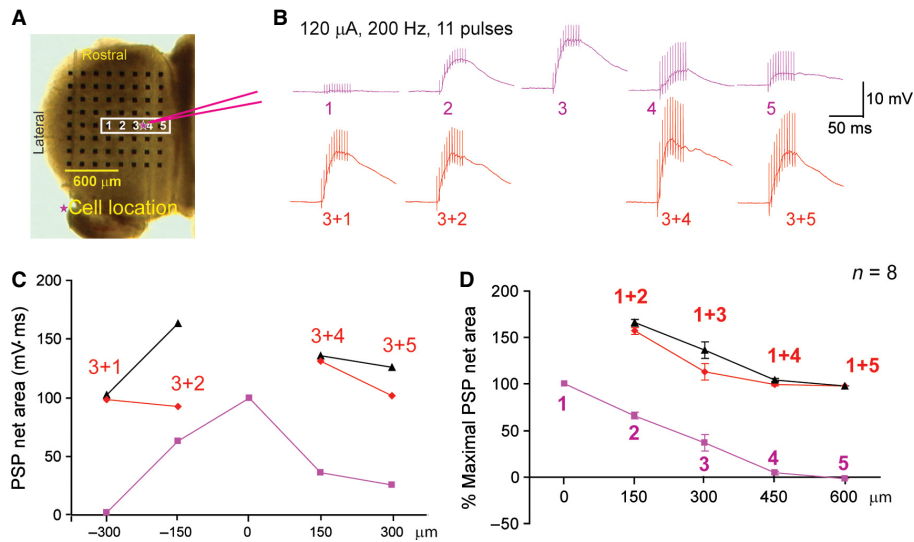


FIG. 10. Effects of simultaneous stimulation of two points on SCi neurons. (A) Arrangement of stimulation electrodes. The location of the example neuron from which the whole cell recording was made is indicated by a pink asterisk. It was close to electrode #3. (B) The effects of single-point stimulation (upper panels in violet) and two-point stimulation (lower panels in red). (C) PSP net area for the data shown in B, plotted against horizontal distance from the recording. Violet lines indicate the effect of single-point stimulation (upper row in B). Red lines indicate the actual data from two-point stimulation. Black lines indicate the algebraic summation. (D) Population data from eight SCi neurons, plotted against horizontal distance, neglecting the medio-lateral polarity. As in C, the violet line indicates the data from the single electrode stimulation, the red line indicates the actual data from the two-point stimulation, and the black line indicates the algebraic sum. There are no significant differences between the actual data and algebraic sum ($P = 0.062$ at $300 \mu\text{m}$).

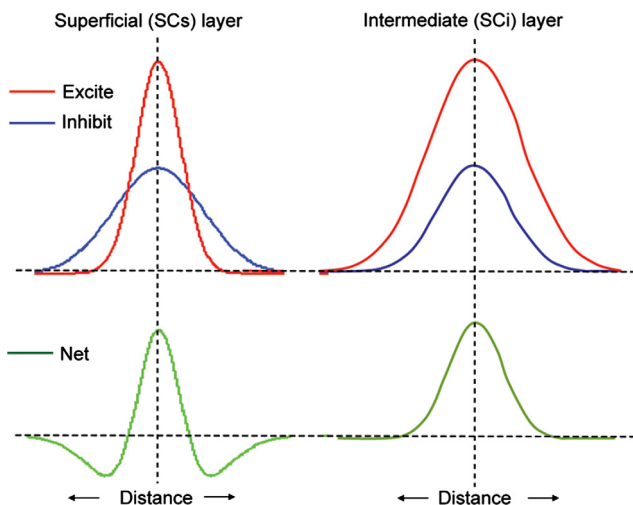


FIG. 11. Schematic diagram explaining our hypothesis of the mechanism underlying the relationship between the responses and distances on the lateral interaction in the SCs and SCi. The excitatory (red) and inhibitory (blue) interactions are shown in the top row, while the net interactions (green) resulting from subtraction of excitatory interactions from inhibitory interactions are shown in the bottom row.

organized for localization of salient stimuli both in the spatial and in the temporal domains. Recently, Mysore & Knudsen (2011) analysed the neural mechanism of saliency detection in the optic tectum of the barn owl *Tyto alba* and showed the critical role of the lateral inhibition *in vivo*. Here, we have demonstrated that this lateral inhibition is also implemented within the mammalian SCs.

Lateral interactions in the SCi

We also identified extensive lateral excitation and inhibition in the Si. However, as shown in Fig. 6, the extent of excitation dominated

that of inhibition, and inhibitory effects were apparently masked. As shown in Fig. 8B and C (right), although the amplitude was smaller than the whole inhibitory response observed before administration of glutamate receptor antagonists, a part of the long-range inhibitory connection was mediated by inhibitory interneurons of long horizontal axons $300\text{--}450 \mu\text{m}$ in length. This is consistent with a previous description of GABAergic SCi neurons with long horizontal axonal projections (Sooksawat *et al.*, 2011). The spatial relationship of excitation and inhibition in the SCi is summarized in Fig. 11 (right).

Our results appear to contradict a previous *in vitro* study (Lee & Hall, 2006), which used photo-stimulation to avoid activation of fibers of passage. This study failed to find long-range excitation or inhibition in the SCi. Because a single short pulse of uncaged glutamate evoked excitatory synaptic responses within a limited range, they concluded that the SCi does not have intrinsic remote inhibition. One possible explanation for such a discrepancy was that the study of Lee & Hall (2006) employed coronal and sagittal slices of SC, which probably cut most of the horizontal connections, to render them ineffective in the slice. In the horizontal slices that we adopted in the present study, these lateral connections were more probably preserved. Another possible explanation is that the majority of long-range lateral inhibition in the SCi is mediated by polysynaptic chains of excitatory transmission connected to local inhibitory neurons (Fig. 8B and D). Such polysynaptic linkages could not be detected in the experiments by Lee & Hall (2006). Regardless, our results obtained by the two-point stimulation techniques (electrical and photo-uncaging of glutamate) in horizontal slices suggest that distant excitatory and inhibitory responses were largely caused by multi-synaptic transmission, and not activation of fibers of passage. The response–distance curves (Fig. 6D, E) for inhibition and excitation in the SCi are very similar. When two different sites in the SCi were stimulated, excitatory responses appeared to be simply summed irrespective of the distance (Fig. 10), which was a marked difference from the SCs. From the temporal aspect, both excitatory and inhibitory responses in the SCi neurons

gradually grew during stimulation and exhibited an increasing synaptic profile (Fig. 7). These results suggest that the lateral interactions in the SCi are more suitable for integrating the inputs added to various locations on the SC map over time.

The precise synaptic mechanisms of lateral inhibition in the SCs and SCi probably differ. In the SCs, the existence of GABAergic presynaptic dendrites has been reported (Mize *et al.*, 1994). In our previous study (Endo *et al.*, 2003), many of the GABAergic horizontal cells in the SCs appeared to lack axons, which suggests that the dendro-dendritic synapses mainly mediate the lateral inhibition in the SCs. In contrast, a population of GABAergic neurons in the SCi issued long horizontal axons (Sooksawate *et al.*, 2011), which suggest that lateral inhibition within the SCi is mediated by axo-dendritic synapses.

Functional differentiation between the SCs and SCi

The striking difference in the local circuit properties between the SCs and SCi suggests very different functions. The SCs is most suitable for change detection both in the temporal and in the spatial domain and would be ideal to signal visual saliency (Itti & Koch, 2001; Boehnke & Munoz, 2008; Mysore & Knudsen, 2011). The SCi circuit is more suitable for temporal and spatial accumulation and integration of the signals added to various locations in visual space. The latter property may be based on the balanced excitation and inhibition in the circuit, and enables the SCi circuit to accumulate information at a subthreshold level for decision-making (Horwitz & Newsome, 2001; Ratcliff *et al.*, 2003). However, as shown in previous studies (Isa *et al.*, 1998; Saito and Isa 2003), the SCi circuit could be switched to non-linear bursting mode, which depends on the activation of NMDA-type glutamate receptors when GABAergic inhibition is reduced. Such reduction in inhibition might be caused either by reduction in extrinsic inhibition from the substantia nigra pars reticulata, zona incerta or mesencephalic reticular formation (Hikosaka & Wurtz, 1983; May & Hall, 1984; Ficalora & Mize, 1989; Appell & Behan, 1990), or reduced excitation of inhibitory interneurons. Moreover, we have recently shown that the inhibitory interneurons in the SCi are innervated directly by GABAergic inputs from the substantia nigra (Kaneda *et al.*, 2008), suggesting the excitation–inhibition balance in the SCi circuit is subject to control by the basal ganglia. Thus, when the balance between excitation and inhibition is changed, the SCi circuit would generate and send bursting activity to the downstream brainstem gaze center to induce the orienting gaze shift (Sparks, 2002). Such a mode-change in the excitation–inhibition balance in the SCi circuit might switch the function of SCi circuits from ‘balanced information accumulator’ to ‘decision-maker’. This hypothesis might reconcile the concurrent debate on the role of lateral interaction in the SCi map in the target selection process (Isa & Saito, 2001; Saito and Isa 2003; Isa & Hall, 2009).

Conclusions

This study clarified that the SC contains two different layers with sharp contrast in the mechanism of signal processing by electrophysiological assessment. The sensory layer (SCs) is optimized to localize the single most salient stimulus and the motor layer (SCi) is optimized to accumulate the information for decision-making. Furthermore, signals are known to be directly transmitted from the sensory layer to the motor layer (Lee *et al.*, 1997; Isa *et al.*, 1998; Helms *et al.*, 2004; Phongphananee *et al.*, 2008). Thus, the SC would represent a typical example of neural machinery, which

enables efficient transformation of the sensory signals into motor commands. Modeling of these processes with the biological parameters obtained in this study is expected to help understand the most fundamental sensory-motor processing for saliency detection.

Acknowledgments

This study was supported by the Human Frontier Science Program (RGP39/2005) and the Grant-in-Aid from the Ministry of Education, Culture, Sports, Science and Technology (Project Nos. 17021041, 18200027) of Japan. D.P.M. was supported by the Canada Research Chair Program.

Abbreviations

APV, (2R)-amino-5-phosphonovaleric acid; CNQX, 6-cyano-7-nitroquinoxaline-2,3-dione; EPSC, excitatory postsynaptic current; EPSP, excitatory postsynaptic potential; IPSC, inhibitory postsynaptic current; IPSP, inhibitory postsynaptic potential; SC, superior colliculus; SCi, intermediate SC; SCs, superficial SC; SO, stratum opticum.

References

- Appell, P.P. & Behan, M. (1990) Sources of subcortical GABAergic projections to the superior colliculus in the cat. *J. Comp. Neurol.*, **302**, 143–158.
- Arai, K., Das, S., Keller, E. & Aiyochi, E. (1999) A distributed model of the saccade system: simulations of temporally perturbed saccades using position and velocity feedback. *Neural Networks*, **12**, 1359–1375.
- Badler, J.B. & Keller, E.L. (2009) Decoding of a motor command vector from distributed activity in superior colliculus. *Biol. Cybern.*, **86**, 179–189.
- Behan, M. (1985) An EM-autoradiographic and EM-HRP study of the commissural projection of the superior colliculus in the cat. *J. Comp. Neurol.*, **234**, 105–116.
- Boehnke, S.E. & Munoz, D.P. (2008) On the importance of the transient visual response in the superior colliculus. *Curr. Opin. Neurobiol.*, **18**, 544–551.
- Buswell, G. (1935) *How People Look at Pictures*. University of Chicago Press, Oxford, UK.
- Dalva, M.B. & Katz, L.C. (1994) Rearrangements of synaptic connections in visual cortex revealed by laser photostimulation. *Science*, **265**, 255–258.
- Dorris, M.C., Olivier, E. & Munoz, D.P. (2007) Competitive integration of visual and preparatory signals in the superior colliculus during saccadic programming. *J. Neurosci.*, **27**, 5053–5062.
- Edelman, J.A. & Keller, E.L. (1998) Dependence on target configuration of express saccade-related activity in the primate superior colliculus. *J. Neurophysiol.*, **80**, 1407–1426.
- Edwards, S.B. (1980) The deep cell layers of the superior colliculus; their reticular characteristics and structural organization. In Hobson, J.A. & Brazier, M.A.B. (Eds), *The Reticular Formation Revisited*. Raven Press, New York, pp. 193–209.
- Endo, T., Yanagawa, Y., Obata, K. & Isa, T. (2003) Characteristics of GABAergic neurons in the superficial superior colliculus in mice. *Neurosci. Lett.*, **346**, 81–84.
- Ficalora, A.S. & Mize, R.R. (1989) The neurons of the substantia nigra and zona incerta which project to the cat superior colliculus are GABA immunoreactive: a double-label study using GABA immunocytochemistry and lectin retrograde transport. *Neuroscience*, **29**, 567–581.
- Gandhi, N.J. & Katnani, H.A. (2011) Motor functions of the superior colliculus. *Annu. Rev. Neurosci.*, **34**, 205–231.
- Godement, P., Salaun, J. & Imbert, M. (1984) Prenatal and postnatal development of retinogeniculate and retinocollicular projections in the mouse. *J. Comp. Neurol.*, **230**, 552–575.
- Helms, M.C., Özen, G. & Hall, W.C. (2004) Organization of the intermediate gray layer of the superior colliculus. I. Intrinsic vertical connections. *J. Neurophysiol.*, **91**, 1706–1715.
- Hikosaka, O. & Wurtz, R.H. (1983) Visual and oculomotor functions of monkey substantia nigra pars reticulata. IV. Relation of substantia nigra to superior colliculus. *J. Neurophysiol.*, **49**, 1285–1301.
- Horwitz, G.D. & Newsome, W.T. (2001) Target selection for saccadic eye movements: prelude activity in the superior colliculus during a direction-discrimination task. *J. Neurophysiol.*, **86**, 2543–2558.
- Isa, T. & Hall, W.C. (2009) Exploring the superior colliculus *in vitro*. *J. Neurophysiol.*, **102**, 2581–2593.

- Isa, T. & Saito, Y. (2001) The direct visuo-motor pathway in mammalian superior colliculus; novel perspective on the interlaminar connection. *Neurosci. Res.*, **41**, 107–113.
- Isa, T., Endo, T. & Saito, Y. (1998) The visuo-motor pathway in the local circuit of the rat superior colliculus. *J. Neurosci.*, **18**, 8496–8504.
- Itti, L. & Koch, C. (2001) Computational modelling of visual attention. *Nat. Rev. Neurosci.*, **2**, 194–203.
- Kaneda, K., Isa, K., Yanagawa, Y. & Isa, T. (2008) Nigral inhibition of GABAergic neurons in mouse superior colliculus. *J. Neurosci.*, **28**, 11071–11078.
- Kaneko, K., Tamamaki, N., Owada, H., Kakizaki, T., Kume, N., Totsuka, M., Yamamoto, T., Yawo, H., Yagi, T., Obata, K. & Yanagawa, Y. (2008) Noradrenergic excitation of a subpopulation of GABAergic cells in the basolateral amygdala via both activation of nonselective cationic conductance and suppression of resting K⁺ conductance: a study using glutamate decarboxylase 67-green fluorescent protein knock-in mice. *Neuroscience*, **157**, 781–797.
- Krauzlis, R.J., Lovejoy, L.P. & Zénon, A. (2013) Superior colliculus and visual spatial attention. *Annu. Rev. Neurosci.*, **36**, 165–182.
- Langer, T.P. & Lund, R.D. (1974) The upper layers of the superior colliculus of the rat: a Golgi study. *J. Comp. Neurol.*, **158**, 418–435.
- Lee, P. & Hall, W.C. (2006) An *in vitro* study of horizontal connections in the intermediate layer of the superior colliculus. *J. Neurosci.*, **26**, 4763–4768.
- Lee, C., Rohrer, W.H. & Sparks, D.L. (1988) Population coding of saccadic eye movements by neurons in the superior colliculus. *Nature*, **332**, 357–360.
- Lee, P.H., Helms, M.C., Augustine, G.J. & Hall, W.C. (1997) Role of intrinsic synaptic circuitry in collicular sensorimotor integration. *Proc. Natl. Acad. Sci. USA*, **94**, 13299–13304.
- Lee, P.H., Sooksawate, T., Yanagawa, Y., Isa, K., Isa, T. & Hall, W.C. (2007) Identity of a pathway for saccadic suppression. *Proc. Natl. Acad. Sci. USA*, **104**, 6824–6827.
- Marino, R.A., Trappenberg, T.P., Dorris, M.C. & Munoz, D.P. (2012) Spatial interactions in the superior colliculus predict saccade behavior in a neural field model. *J. Cognitive Neurosci.*, **24**, 315–336.
- May, P.J. & Hall, W.C. (1984) Relationships between the nigroretectal pathway and the cells of origin of the predorsal bundle. *J. Comp. Neurol.*, **226**, 357–376.
- Meredith, M.A. & Ramoa, A.S. (1998) Intrinsic circuitry of the superior colliculus: pharmacophysiological identification of horizontally oriented inhibitory interneurons. *J. Neurophysiol.*, **79**, 1597–1602.
- Mize, R.R. (1992) The organization of GABAergic neurons in the mammalian superior colliculus. *Prog. Brain Res.*, **90**, 219–248.
- Mize, R.R., Whitworth, R.H., Nunes-Cardozo, B. & van der Want, J. (1994) Ultrastructural organization of GABA in the rabbit superior colliculus revealed by quantitative postembedding immunocytochemistry. *J. Comp. Neurol.*, **341**, 273–287.
- Munoz, D.P. & Istvan, P.J. (1998) Lateral inhibitory interactions in the intermediate layers of the monkey superior colliculus. *J. Neurophysiol.*, **79**, 1193–1209.
- Mysore, S.P. & Knudsen, E.I. (2011) The role of a midbrain network in competitive stimulus selection. *Curr. Opin. Neurobiol.*, **21**, 653–660.
- Olivier, E., Corvisier, J., Pauluis, Q. & Hardy, O. (2000) Evidence for glutaminergic tectoretectal neurons in the cat superior colliculus: a comparison with GABAergic tectoretectal neurons. *Eur. J. Neurosci.*, **12**, 2354–2366.
- Phongphanphane, P., Kaneda, K. & Isa, T. (2008) Spatiotemporal profiles of field potentials in mouse superior colliculus analyzed by multichannel recording. *J. Neurosci.*, **28**, 9309–9318.
- Ratcliff, R., Cheria, A. & Segraves, M. (2003) A comparison of macaque behavior and superior colliculus neuronal activity to predictions from models of two-choice decisions. *J. Neurophysiol.*, **90**, 1392–1407.
- Robinson, D.A. (1972) Eye movements evoked by collicular stimulation in the alert monkey. *Vision Res.*, **12**, 1795–1808.
- Saito, Y. & Isa, T. (2003) Local excitatory network and NMDA receptor activation generate a synchronous and non-linear bursting command from the superior colliculus. *J. Neurosci.*, **23**, 5854–5864.
- Schiller, P.H. & Stryker, M. (1972) Single-unit recording and stimulation in superior colliculus of the alert rhesus monkey. *J. Neurophysiol.*, **35**, 915–924.
- Sooksawate, T., Saito, Y. & Isa, T. (2005) Electrophysiological and morphological properties of identified crossed tecto-reticular neurons in the rat superior colliculus. *Neurosci. Res.*, **52**, 174–184.
- Sooksawate, T., Isa, K., Behan, M., Yanagawa, Y. & Isa, T. (2011) Organization of GABAergic inhibition in the motor output layer of the superior colliculus. *Eur. J. Neurosci.*, **33**, 421–432.
- Sparks, D.L. (1986) Translation of sensory signals into commands for control of saccadic eye movements: role of primate superior colliculus. *Physiol. Rev.*, **66**, 118–171.
- Sparks, D.L. (2002) The brainstem control of saccadic eye movements. *Nat. Rev. Neurosci.*, **3**, 952–964.
- Takahashi, M., Sugiuchi, Y. & Shinoda, Y. (2007) Commissural mirror-symmetric excitation and reciprocal inhibition between the two superior colliculi and their roles in vertical and horizontal eye movements. *J. Neurophysiol.*, **98**, 2664–2682.
- Tamamaki, N., Uhlrich, D.J. & Sherman, S.M. (1995) Morphology of physiologically identified retinal X and Y axons in the cat's thalamus and mid-brain as revealed by intraaxonal injection of biocytin. *J. Comp. Neurol.*, **354**, 583–607.
- Tamamaki, N., Yanagawa, Y., Tomioka, R., Miyazaki, J., Obata, K. & Kaneko, T. (2003) Green fluorescent protein expression and colocalization with calretinin, parvalbumin, and somatostatin in the GAD67-GFP knock-in mouse. *J. Comp. Neurol.*, **467**, 60–79.
- Trappenberg, T.P., Dorris, M.C., Munoz, D.P. & Klein, R.M. (2001) A model of saccade initiation based on the competitive integration of exogenous and endogenous signals in the superior colliculus. *J. Cognitive Neurosci.*, **13**, 256–271.
- Vokoun, C.R., Jackson, M.B. & Basso, M.A. (2010) Intralaminar and interlaminar activity within the rodent superior colliculus visualized with voltage imaging. *J. Neurosci.*, **30**, 10667–10682.
- Vokoun, C.R., Jackson, M.B. & Basso, M.A. (2011) Circuit dynamics of the superior colliculus revealed by *in vitro* voltage imaging. *Ann. NY Acad. Sci.*, **1233**, 41–47.
- White, B.J. & Munoz, D.P. (2011) Separate visual signals for saccade initiation during target selection in the primate superior colliculus. *J. Neurosci.*, **31**, 1570–1578.
- Yarbus, I.A. (1967) *Eye Movements and Vision*. Plenum Press, New York.